

Article

Laser Inter-Satellite Link Visibility and Topology Optimization for Mega Constellation

Qinyu Zhu, Haicheng Tao, Yanhua Cao and Xinhong Li *

School of Information and Communication Engineering, Space Engineering University, Beijing 101416, China; qyzhu97@foxmail.com (Q.Z.); homerthc@foxmail.com (H.T.); yhcao@sina.com (Y.C.)

* Correspondence: 13366159269@189.cn

Abstract: In this paper, we begin by describing the Starlink constellation's configuration plan, treating each satellite as a network node, naming and numbering the various nodes, and then classifying the laser interstellar links (LISLs) according to their orbital alignment and whether they are permanently visible. Whereupon, the method for calculating the respective theoretical interstellar distances required for establishing LISLs under two distinct orbital scenarios, co-orbital and hetero-orbital are analyzed, and the optimal phasing factors are proposed by solving an optimization algorithm for the shortest distance. The OneWeb and Starlink constellations, as well as the constellation states of various phasing factors are simulated, respectively. The Starlink constellation with $F = 11$ obtains the best coverage between 60° north and south latitudes predicated upon the analysis of the constellation N Asset Coverage. Following that, the first phase of the Starlink constellation deployment was modeled in order to analyze and count the number of permanent LISLs in orbit, adjacent to, and nearby. Subsequently, the characteristics of azimuthal, elevation, and range (AER) were subsequently analyzed to ascertain their variation law and to compile the number of permanent and temporary LISLs that could be established at various inter-distance ranges. Finally, predicated on the simulation results, the optimal LISLs connection strategy for the Starlink constellation is evaluated and a static topology for the constellation is constructed.



Citation: Zhu, Q.; Tao, H.; Cao, Y.; Li, X. Laser Inter-Satellite Link Visibility and Topology Optimization for Mega Constellation. *Electronics* **2022**, *11*, 2232. <https://doi.org/10.3390/electronics11142232>

Academic Editor: Manuel Arrebola

Received: 14 June 2022

Accepted: 14 July 2022

Published: 17 July 2022

Publisher's Note: MDPI stays neutral with regard to jurisdictional claims in published maps and institutional affiliations.



Copyright: © 2022 by the authors. Licensee MDPI, Basel, Switzerland. This article is an open access article distributed under the terms and conditions of the Creative Commons Attribution (CC BY) license (<https://creativecommons.org/licenses/by/4.0/>).

Keywords: laser interstellar links; Starlink constellation; phasing factors; N Asset Coverage; visibility analysis

1. Introduction

Satellite networks, as a vital component of 5G and future 6G technologies, already play a pivotal role in aerospace, industrial and agricultural development, transportation, rescue and disaster relief, and smart city construction, among other applications. Mankind's desire for robust communication capabilities and ubiquitous service coverage is driving satellite networks toward increased dynamics, densification, and heterogeneity [1]. The future satellite network will be a colossal multi-layer heterogeneous satellite constellation, posing significant challenges to the network's reliability and scalability, and to the connectivity of the network topology [2].

The construction of the space segment of Iridium's next-generation Iridium system, which includes sixty-six LEO satellites and nine spare satellites, is nearly complete with the launch of the final ten satellites into orbit in January 2019 [3]. In addition, SpaceX devised the Starlink plan in early 2015, which was essentially acknowledged as a link scheme through satellites [4]. As of March 2021, SpaceX's public filings with the Federal Communications Commission (FCC) identify only a few specific constellation parameters, and specify that each satellite will have four laser links, but make no mention of a mechanism for allocating inter-satellite link connections [5]. As the world's largest low-Earth orbit (LEO) constellation to date, with thousands of satellites launched in the first phase alone, the deployment of interstellar link technology offers the potential to alleviate congestion on the ground network and minimize the need for ground stations.

Table 1 outlines the parameters of several typical international LEO constellation systems. It is evident that microsatellite technology tends to be practical, and the fact that a large number of mature commercial-grade components are used to construct microsatellites leads to its short development cycle and low cost [6]. The LEO constellation system has reached its pinnacle of development due to the high demand for high-capacity, low-latency satellite communications [7]. For the development of the next LEO mega-constellations, it is thus crucial to synthesize the variation laws of LISLs in different situations and optimize the static topology of the constellation.

Table 1. Parameters comparison of several typical international LEO satellite constellation systems.

Constellation Name	Orbital Altitude	Start Year	Number of Satellites	Orbit Inclination	Frequency Band
Globalstar	1414 km	2007	48 + 8	52°	L, S, C
Orbcomm 2	825 km	2012	35	45°	V
Iridium NEXT	780 km	2017	66 + 9	86.4°	L, Ka
OneWeb	1200 km	2019	720	87°	Ka, Ku, V
Telesat	1000/1200 km	2023	298	99.5° / 37.4°	Ka
Starlink *	340/550/1150 km	2024	42,000	53°	Ka, Ku, V

* The data of the above satellites are available in the link "<https://www.space-track.org/>" (accessed on 15 April 2020), and the data is updated in real time.

This paper examines, from a topological standpoint, the use of satellites as network nodes and wireless links as network edges, both of which can connect users in the three fields of sea, land, and air through inter-satellite and satellite-ground links [8]. To optimize the topology of OISLs for future navigation satellites, for instance, Zeng et al. proposed the multi-objective discrete binary particle swarm optimization algorithm, which fully took into account the complex constraints of inter-satellite links [9]. Through the analysis of ISL paths, Chen et al. sought to offer insights into the topology and routing design of Mega-constellation networks; numerical results reveal the superiority of optimizing the constellation phasing factor [10]. Consequently, it is worthwhile to investigate the static topology of satellite networks, as well as the optimal phasing factor and connection strategies for LISLs in varying states.

While many researchers have studied and found sufficient performance with the topology design of LEO constellation networks, they frequently base their findings on the assumption that the total number of satellites would not exceed 100, as is the case with the optimal Walker constellation's topology design [11]. As a result, the previously proposed topology algorithms are incompatible with large constellations, and a new link allocation strategy is necessary to re-propose the inter-satellite links in large-scale LEO satellite constellations so as to design an appropriate topology and minimize inter-satellite communication delay [12]. As such, this paper explores the visibility law of the interstellar link layer and proposes connection strategies for characterization and construction of scalable and connected intra-layer topologies for spatial information network topologies utilizing Starlink constellation as an example.

The remaining sections of this paper are structured as follows: In Section 2, an overview of Free-space optics is presented along with the Starlink constellation configuration plan. Section 3 describes the universal geometric approach for optimal inter-satellite visibility. Section 4 reveals the simulation results using the proposed strategy and the variation laws. Finally, this work is concluded in Section 5.

2. Background

Optical wireless communication in space information networks is conventionally referred to as free-space optics (FSO), which refers to optical communication systems that transmit optical signals through the atmosphere rather than through optical fibers, and is a hybrid of fiber optic and wireless communication. FSO links are used to transmit optical signals from an optical transmitter through the atmosphere or space vacuum to

an optical receiver. The transmitter and receiver require a clear line of sight. A satellite laser interplanetary link communication system is illustrated in Figure 1. The system is comprised of an optical subsystem, an ATP subsystem, a communication subsystem, and an interface and control subsystem [13].

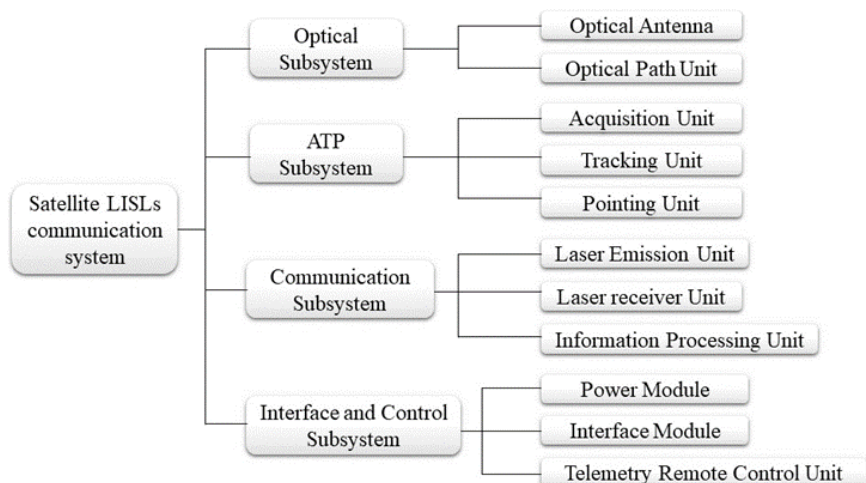


Figure 1. Satellite LISLs communication system.

Laser intersatellite links (LISLs) will be widely used in constellations after deployment in the coming years, such as the first phase of SpaceX's planned Starlink constellation, in which satellites can establish laser connections to other satellites in the same or different orbital planes (OPs). Satellites in this LEO layer constellation can establish laser links with other satellites in the same or different orbital planes. In comparison to conventional microwave communication, laser communication benefits from high transmission rates, wide band-width availability, strong anti-electromagnetic interference capability, high security and confidentiality, as well as the small size, light weight, and low power consumption of laser terminals, all of which contribute to LISLs gradually becoming an important means of establishing future LISLs, and one of the best ways to address the problems of high-speed space communication [14]. However, LISLs do pose several limitations. Due to the narrow beam, it is difficult to target and capture the orbit of LISLs under the high dynamic motion conditions of two satellites, which compounds the complexity of the system design [15].

These studies are crucial for expanding routing options, enhancing satellite redundancy backup, and enhancing satellite networks' topological resilience. Additionally, in order to find reliable temporary LISLs for next-generation optical wireless satellite networks, it is necessary to develop efficient ATP systems with reasonable packet conversion and low cost. Additionally, will be necessary to equip satellites with more optional LISL terminals in order to construct a robust network topology using permanent LISLs and flexible options for a large number of variable temporary LISLs.

Starlink Constellation Configuration Plan

As of January 2022, SpaceX had launched a total of 35 Starlink satellites employing the Falcon-9 launcher, and with the launch of the latest batch, its total number of satellites has increased to 2042, with three orbital types: non-polar inclined orbit, polar orbit, and sun-synchronous orbit, each with an orbital inclination of 53° , 70° , or 97.5° [16]. Since 2014, when SpaceX announced the Starlink constellation initiative, the satellite configuration plan has been revised multiple times. In November 2018, SpaceX proposed amending the FCC's license to lower the LEO layer constellation's orbital altitude from 1150 km to 550 km and to operate 1584 satellites at this altitude [17]. In April 2020, SpaceX amended the FCC license once more, increasing the orbital altitude of all satellites in the LEO layer constellation to 540–570 km, as shown in Table 2.

Table 2. Modified Starlink Constellation Phase I configurations.

Orbit Type	Orbital Altitude	Orbit Inclination	Number of Orbital Planes	Number of Satellites per Orbital Plane	Total
LEO *	550 km	53°	66	24	1584
	540 km	53.2°	66	24	1584
	570 km	70°	36	20	720
	560 km	97.5°	6	58	348
	560 km	97.5°	4	43	172
VLEO	345.6 km	53°			2547
	340.8 km	48°			2748
	335.9 km	42°			2493

* The above orbital data concerning Starlink Constellation Phase I are derived from the FCC reports and the detailed parameters of the Union of concerned scientists satellite database. <https://www.ucsusa.org/nuclear-weapons//space-weapons/satellite-database> (accessed on 1 January 2022).

The Starlink constellation of LISLs terminals has been under continuous development and is expected to eventually provide capacities of up to 10 Gb/s. To accomplish SpaceX's goal of establishing an efficient communications network with global coverage in space, inter-satellite links are required to provide transmission capacity measured in gigabits per second capacity, which will eventually expand to terabits per second, which is the development plan of the next-generation satellite network [18].

3. Methodology and Analytical Approach

3.1. Numbering and Classification of Inter-LISLs

In order to facilitate description, this paper unifies the orbits and satellites within the orbits of the Walker constellation by naming the satellite nodes in the form of $S(P_i, M_j)$, indicating the M_j satellite within the first P_i orbital plane. The orbit number P_i increases in clockwise direction, and the satellite number M_j increases in the same direction as the orbit. The orbits P_{i+1} and P_{i-1} are named as adjacent orbits of P_i , since the satellites in the same orbit have the same orbital speed and direction, M_{j+1} and M_{j-1} are named as the forward and backward satellites of M_j , respectively.

The classification of LISLs for the mega-constellation is based on two different rubrics: whether the LISLs are in the same orbit, and whether the LISLs are permanently visible.

1. Co-orbiting and hetero-orbiting LISLs

In an orbital plane, satellites with the same orbital altitude all move in the same direction at identical speed. According to the positions of satellites within the constellation, LISLs within the constellation can be classified into two main types: (a) LISLs established between two satellites in the same orbital plane; (b) LISLs established between different orbital planes.

Among them, the heterodyne LISLs can be further classified into the following three types:

- Adjacent OP LISLs, which are between satellites in adjacent OPs;
- Neighboring non-adjacent OP LISLs, which are between satellites in nearby instead of adjacent OPs;
- Crossing OP LISLs, which are between satellites in crossing OPs.

As shown in Figure 2a, an example of adjacent and nearby OP LISLs, where the satellite $S(1,1)$ has a LISL indicated by a yellow dashed line, and the satellites $S(2,65)$ and $S(24,35)$ are located in two nearby planes, P_2 and P_{24} , respectively; An example of crossing OP LISLs is shown in Figure 2b, where satellites $S(12,32)$ and $S(14,21)$ are located in orbital planes P_{12} and P_{14} , respectively, both intersecting with P_1 where $S(1,1)$ is located.

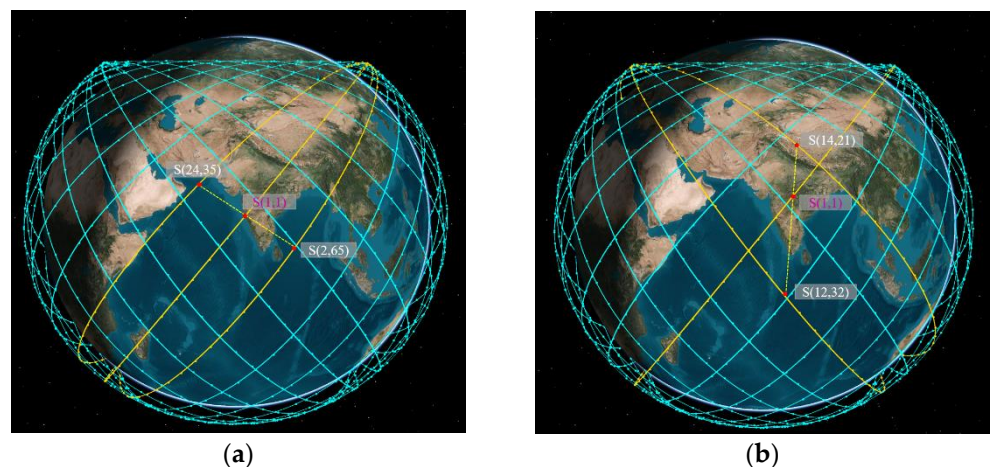


Figure 2. This is the schematic diagram of heterodyne LISLs. (a) Adjacent and nearby OP LISLs; (b) Crossing OP LISLs.

2. Permanent and temporary LISLs

Intersatellite links can be classified as permanent and temporary LISLs, also referred to as static and dynamic LISLs, depending on the duration of their connection. Permanent and temporary inter-satellite links are determined by the relative positions and motion relationships between satellites in the constellation, i.e., the geometric configuration of the constellation, the relevant performance parameters of the antennas, the phase difference, and the azimuth. These parameters also serve as the main parameters describing the satellite communication link. Permanent interstellar links are always connected and do not have to be dynamically reconstructed, while temporary interstellar links are often dynamically disconnected and dynamically reconstructed [19].

Permanent LISLs established between satellites orbiting at the same speed within the same orbital plane are relatively simple to upkeep; between neighboring satellites orbiting at different speeds within the same orbital plane, there are some difficulties in establishing permanent LISLs due to the relative speeds, but over time, a large number of temporary LISLs are generated within different time slices. For instance, when observing the Starlink constellation from any region above the Earth, half of the constellation's satellites can be seen orbiting toward the southeast while the other half orbit toward the northeast. These satellites on mission generate a large number of intermittent LISLs between the crossed orbital planes. While this connection state cannot last for an extended period of time, such a link is essential for increasing the constellation redundancy and resistance to destruction, improving the routing options and thus reducing the path delay. As a result, determining the pattern of interstellar links between orbits at various stages of the cycle is an especially intriguing task for enhancing the flexibility of network communication.

3.2. Initial Phase

After the satellites are assigned their numbers, their spatial position information can be visually observed and analyzed, as shown in Figure 3, a schematic diagram of the distribution of satellites in the Delta constellation. At this time, the satellites in three different orbital planes are all climbing at speed v in the ascending orbital segment. Taking $S(1, 1)$ as the initial position, assuming that the constellation is uniform, and the inclination of all orbital planes in the constellation relative to the equator is the same, the initial phase of any satellite M_j on any orbit P_i in the constellation τ is shown in Equation (1).

$$\tau = (-2\pi \times F \times (P_i - 1)) / S + (2\pi \times (M_j - 1)) / M \quad (1)$$

where $\Delta\sigma$ is the phase difference of adjacent satellites in the same orbital plane; $\Delta\Omega$ is the phase difference of the ascending intersection point of two adjacent orbital planes; and $\Delta\omega$

is the phase difference between two neighboring satellites in adjacent orbital planes, as shown in Equations (2)~(4), respectively.

$$\Delta\sigma = 2\pi/M \quad (2)$$

$$\Delta\Omega = 2\pi/P \quad (3)$$

$$\Delta\omega = 2\pi \times F/S \quad (4)$$

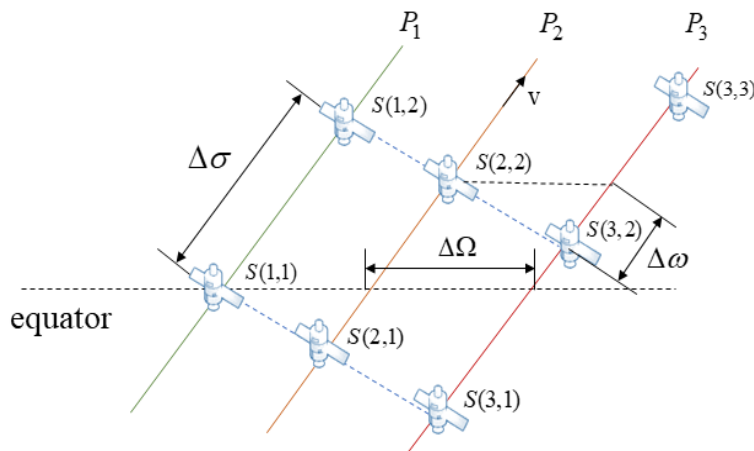


Figure 3. Distribution of satellites in the Delta constellation.

3.3. Chain Building Threshold Analysis

The mega-constellation features relative motion between satellites, constant visibility changes between satellites in different orbits, and inter-satellite links are also opened and closed, resulting in a highly dynamic and time-varying spatial information network. In general, LISLs adopt the principle of continuous link building to establish an intersatellite network topology comprised of fixed pairs in spatial position relationships. Due to the fact that LISLs require pre-captured antennas, and the process of aligning antennas for correction takes a significant amount of time, fixed pairing can greatly reduce link switching and the time required for antenna alignment [20]. Based on the continuous regime of LISLs, it is prerequisite and essential to analyze the constellation network topology by evaluating the visibility relationship for each satellite in order to calculate the spatial position and inter-satellite distance of satellites in the constellation, as well as to select the appropriate satellites for link building between co-orbital and hetero-orbital links [21].

1. Calculation of the distance of LISLs within the same orbit

If there are satellites S_1 and S_2 in the same orbit then the distance between the two satellites d_{12} is shown in Equation (5).

$$d_{12} = \sqrt{2} \times (R + h) \times \sqrt{1 - \cos\angle s_1 o s_2} \quad (5)$$

where d_{12} denotes the distance between satellites S_1 and S_2 , R is the radius of the Earth, h is the orbital altitude of satellites S_1 and S_2 , γ is half of the corresponding geocentric angle of satellites, and $\angle s_1 o s_2$ is the angle between satellites S_1 and S_2 . The radius of the Earth at its equator is approximately 6378 km, as shown in Figure 4, where the blue segment represents the Earth, the gray segment represents the atmosphere, and the yellow segment represents any satellite in the LEO layer. As a result of the previous analysis, it is evident that satellites in the same orbit remain relatively stationary throughout the operation, the link length formed is constant, and the azimuth and elevation angles do not change significantly, so it is relatively easy to establish LISLs. However, additional factors need to be taken into consideration regarding the satellite communication links, such as the satellites S_1 and S_3 in Figure 4 being at one time blocked by the Earth for communication links; the scattering

and absorption of various gases and other suspended particles in the Earth's atmosphere, and the influence of atmospheric turbulence, which can cause the laser communication links of the constellation to be attenuated, which may manifest as light intensity flicker, beam drift, and jitter [22]. Therefore, for co-orbital satellites to establish link connections, it is necessary for the conditions shown in Equation (6) to be met.

$$(R + h) \times \cos\gamma > (R + H) \quad (6)$$

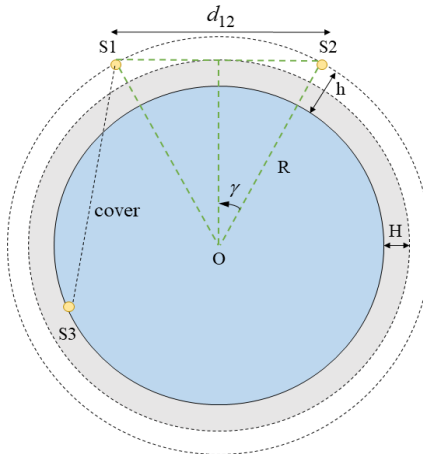


Figure 4. Scenario of establishing LISLs between the same orbit.

2. Distance calculation of LISLs between different orbits

The angle formed between the two satellites and the center of the earth θ can be calculated from the satellite's latitude and longitude position information, and the equation for the geocentric angle of satellites S_1 and S_2 is shown in (7).

$$\theta = \arccos[\sin(\varphi_1) \times \sin(\varphi_2) + \cos(\varphi_1) \times \cos(\varphi_2) \times \cos(\lambda_1 - \lambda_2)] \quad (7)$$

where φ_1 is latitude and λ_1 is longitude, the position information of the satellite S_1 can be noted as (φ_1, λ_1) ; the satellite geographic location coordinates formula is shown in (8)~(10).

$$\varphi_1 = \arcsin(\sin(i) \times \sin(\beta)) \quad (8)$$

$$\lambda_1 = \lambda_0 + \arctan(\cos(i) \times \tan(\beta)) - \zeta \times t + C \quad (9)$$

$$\beta = \omega \times t + \tau \quad (10)$$

where i is the orbital inclination, β is the angular distance between the satellite S_1 and the ascending node, λ_0 is the longitude of the ascending node, ζ is the angular velocity of the Earth's rotation, t is the time of the satellite, ω is the angular velocity of the satellite, which is generally determined by the satellite period, τ is the initial phase of the satellite, which is calculated by Equation (1). When C is a constant, $\beta \in [-\pi, -\pi/2]$, $C = -\pi$; when $\beta \in [-\pi/2, \pi/2]$, $C = 0$; when $\beta \in [\pi/2, \pi]$, $C = \pi$.

As shown in Figure 5, the instantaneous elevation angles of the satellites S_1 and S_2 are δ_1 and δ_2 , respectively; and the elevation angle is the angle between the tangent line of the satellite's orbit and the LISLs. Based on the geocentric angle θ , the instantaneous interplanetary link distance d_{12} , and the instantaneous elevation angles δ_1 and δ_2 can be calculated from the satellites S_1 and S_2 , as shown in Equations (11)~(13).

$$d_{12} = \sqrt{R_1^2 + R_2^2 - 2 \times R_1 \times R_2 \times \cos\theta} \quad (11)$$

$$\delta_1 = \arccos(R_2 \times \sin(\theta) / d_{12}) \quad (12)$$

$$\delta_2 = \arccos(R_1 \times \sin(\theta) / d_{12}) \quad (13)$$

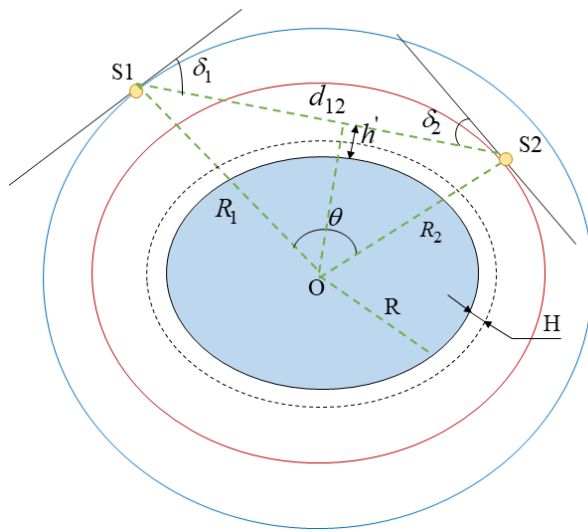


Figure 5. Establishment of instantaneous LISLs between different orbits.

The altitude of the LISLs established by the two satellites above the surface h' is shown in Equation (14).

$$h' = R_1 \times \cos(\delta_1) \quad (14)$$

Since the radius R_i of the satellites in the same orbital plane are identical, which is $R_i = R + h$, the instantaneous inter-satellite link between the two satellites d is therefore presented in Equation (15).

$$d = \sqrt{2 \times R^2 \times (1 - \cos\theta)} \quad (15)$$

The maximum visible distance x between the two satellites is shown in Equation (16).

$$x = 2 \times \sqrt{R_i^2 - (R + H)^2} \quad (16)$$

When $h' > R + H$ or $d < x$, an interplanetary link can be established between the satellites S_1 and S_2 , but not vice versa, so the set of visible satellites of the satellite S_1 can be expressed as $Y = \{S_1 | x \geq d_{li}\}$.

3.4. Optimal Phasing Factor

After the initial phase in the constellation is determined using Formula (1), the longitude and latitude coordinates of the satellite are determined using Formulas (8) and (9), and the distance between satellites in different orbits is calculated by the Formula (15), which is then substituted into Formula (16), to obtain the longest visible distance x between the two satellites. Using x as the criterion, if the maximum value is not exceeded, it means that the two satellites are within the visible range of each other and LISLs can be established [23]. From the above analysis, the phasing factor indicates the relative phase difference of satellites passing through the equatorial plane between adjacent orbits, which is the relative phase measured by the interval $1/P$ of adjacent satellites in any one orbit. Therefore, the first step in simulation modeling is to solve the phase between satellites adopting an optimization algorithm. Two fundamental criteria govern the optimization process are: first, to maximize the shortest distance between any orbiting satellites; and second, in the case of establishing LISLs in cross orbital planes, no collision event between satellites in different orbital planes can occur [24]. The above rule is also acknowledged as the binomial criterion.

This paper calculates the shortest distance between any two satellites at different times by simulating the situation under different phasing factors. Using an optimization algorithm to find the optimal solution that meets the conditions, its N Asset Coverage is analyzed, and the pros and cons of the constellation performance are compared [25].

For the Walker constellation, a five-element parameter set can be applied to fully describe its configuration: $\{M, P, F, h, i\}$, which indicates that the constellation consists of S satellites evenly distributed in P orbital planes, h is the orbital altitude, i is the orbital inclination, M is the number of satellites contained in each orbit. Accordingly, the total number of satellites is $S = P \times M$, F indicating the phase value of the eastern orbit ahead of the western orbit, which is related to the total number of satellites, and the value range is $0 \leq F \leq P - 1$. The pseudo code for the algorithm is shown in Algorithm 1.

Algorithm 1 Pseudocode for optimal phasing factor solution algorithm

```

Input: P
Output: Optimal Phasing Factor
1: Max ← 0, Min ← 0, BF ← 0
2: for F ← 0 To  $P_i - 1$ 
3:   for M ← 1 To  $M_j$ 
4:     for N ← 1 To M
5:       d12 ← Calculate the distance of LISLs for  $S_1$  and  $S_2$  using Equation (12)
6:       if Min == 0 Then
7:         Min ← d12
8:       else
9:         if Min < d12 hen Min ← d12 End
10:      end
11:    Next N
12:  Next M
13:  if Max < Min Then
14:    Max ← Min
15:  end
16: Next P
17: F = P - 1
18: Optimal Inter Spacing ← F
  
```

4. Results and Discussion

4.1. Solving for the Optimal Phasing Factor

Based on the constellation data in Table 1, it can be observed that the Starlink constellation and the OneWeb constellation are expected to deploy a large number of satellites, whereas other constellations such as Telesat are not in the same order of magnitude; therefore, no comparison is produced. This paper examines the variation of the shortest distance under various phasing factors for the OneWeb and Starlink constellations, as depicted in Figure 6.

Figure 6a illustrates the variation of the OneWeb constellation, where $0 \leq F \leq 17$, due to the absence of cross-links, the shortest distance of LISLs is always greater than 0, collisions do not occur, and the shortest distance appears when $F = 9$. Figure 6b shows the variation of the Starlink constellation, where $0 \leq F \leq 23$, when the shortest distance of LISLs is 0, the two satellites will collide, thereby even values of F should be avoided. In order to satisfy the two basic optimization criteria, it is necessary to select the peak value so that the optimal F for the LEO layer in the first phase of the Starlink constellation is obtained as 11 by solving.

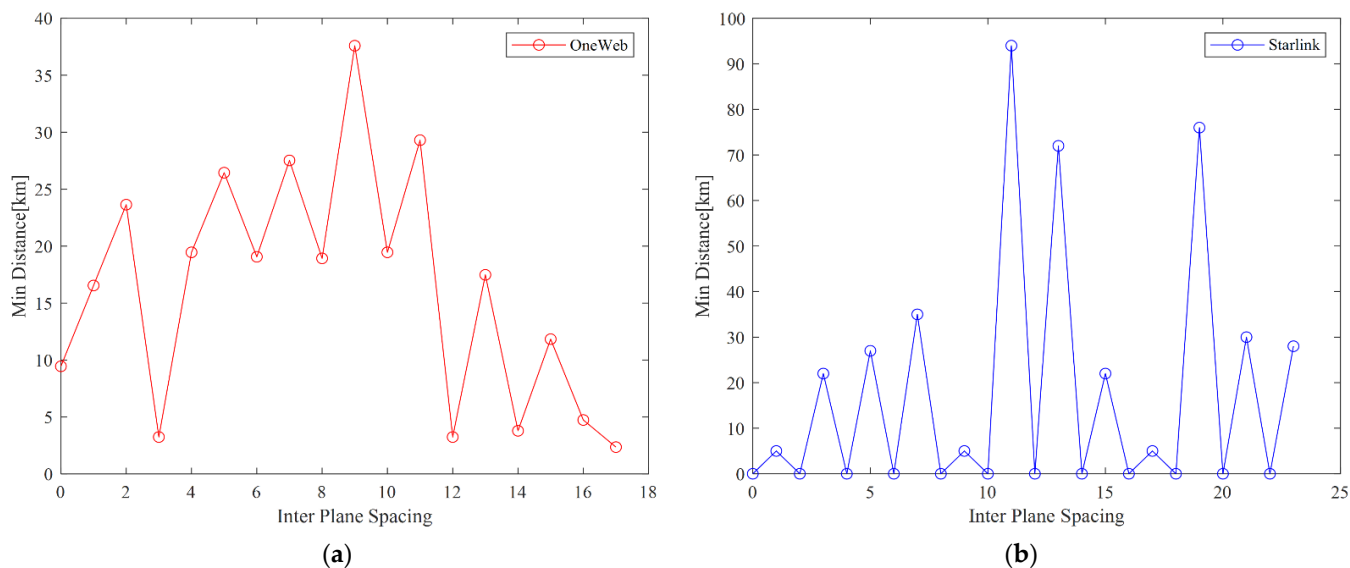


Figure 6. Solving for the optimal Phasing Factor. (a) The variation of the OneWeb constellation, where $0 \leq F \leq 17$; (b) The variation of the Starlink constellation, where $0 \leq F \leq 23$.

4.2. Simulation Modeling

As shown in Figure 7a, which is the LEO layer of the OneWeb constellation, and the simulation's five-element parameter set is $\{40, 18, 9, 1200 \text{ km}, 86.4^\circ\}$, with 18 orbital planes and 40 satellites per orbit, and the optimal phasing factor is set to 9. As shown in Figure 7b, which is the LEO layer of the Starlink constellation, the simulation's five-element parameter set is $\{66, 24, 11, 550 \text{ km}, 53^\circ\}$, with 24 orbital planes and 66 satellites per orbit, also the optimal phasing factor is set to 11. In the simulation figure, satellites of the same color represent that they are in the same orbit. The effects of various satellite numbers and phasing factors on the coverage performance are discussed using the OneWeb constellation as a comparison group. The simulation begins at 4:00:00.000 on 1 July 2022 and ends at 4:00:00.000 on 2 July 2022, lasting 24 h.

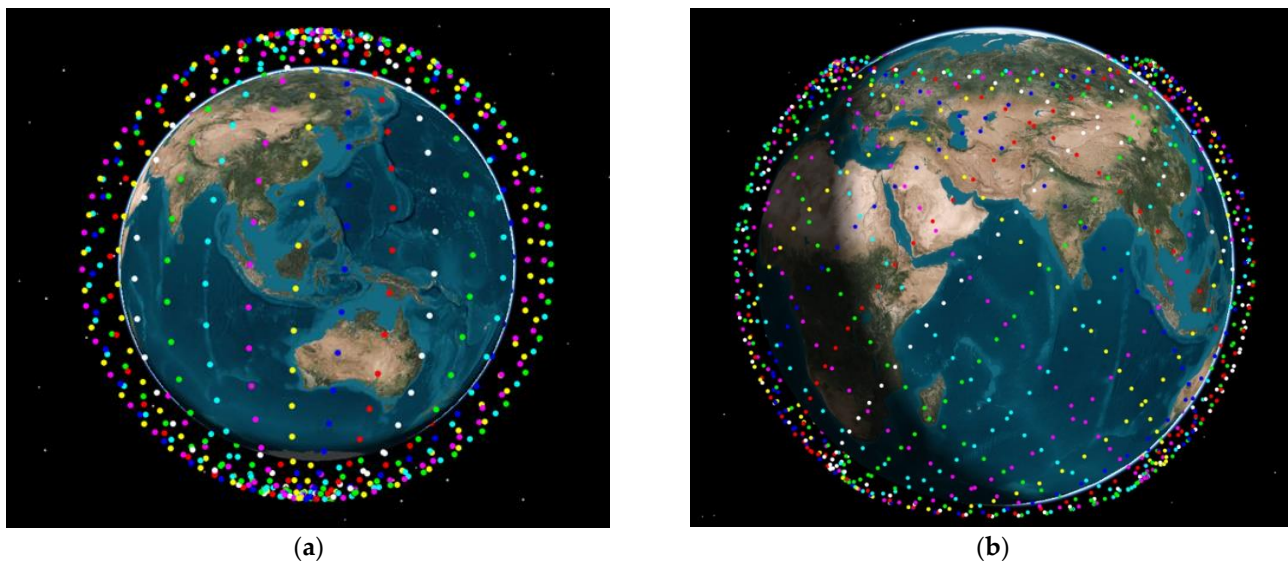


Figure 7. Modeling diagram of Starlink and OneWeb constellation (Data on the orbits of satellites in the constellation are detailed in the link in the Supplementary Materials). (a) OneWeb constellation; (b) Starlink constellation.

4.3. Comparison of Coverage Performance

This paper establishes four groups of coverage performance comparisons and provides the global coverage of the Starlink and OneWeb constellation. Figure 8a is the Starlink constellation with $F = 1$, Figure 8b represents the Starlink constellation with $F = 11$, Figure 8c represents the OneWeb constellation with $F = 1$, and Figure 8d represents the OneWeb constellation with $F = 9$. From the graph analysis, the following conclusions can be drawn:

- OneWeb's constellation of 720 satellites essentially provides global coverage, with polar regions receiving optimal coverage. Between 60° north and south latitude, when $F = 1$, the constellation N Asset Coverage is up to 85; when $F = 9$, the constellation N Asset Coverage is up to 90. In polar regions, when $F = 1$, the constellation N Asset Coverage is up to 110; when $F = 9$, the constellation N Asset Coverage is up to 130.
- The 1584 satellites in the first phase of Starlink have not yet covered all polar regions; optimal coverage can be achieved between $30^\circ \sim 50^\circ$ north and south latitude. Between 60° north and south latitudes, when $F = 1$, the constellation N Asset Coverage is up to 85; when $F = 11$, the constellation N Asset Coverage is up to 130. The 0-fold coverage in the region above 60° north-south latitude is determined by the orbital inclination, and the coverage will be enhanced by the deployment of an orbital surface with an inclination of 97.5° .

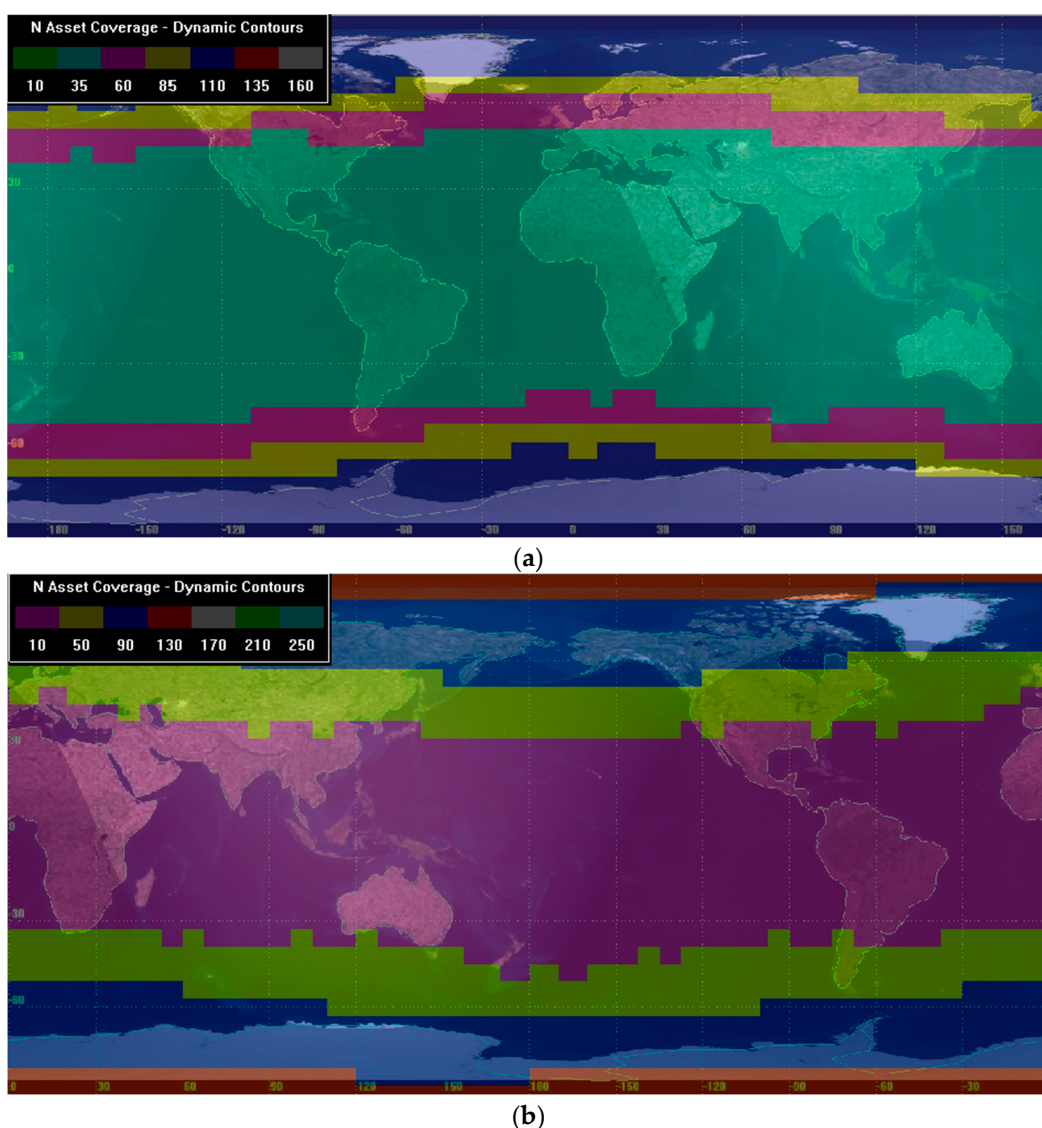


Figure 8. Cont.

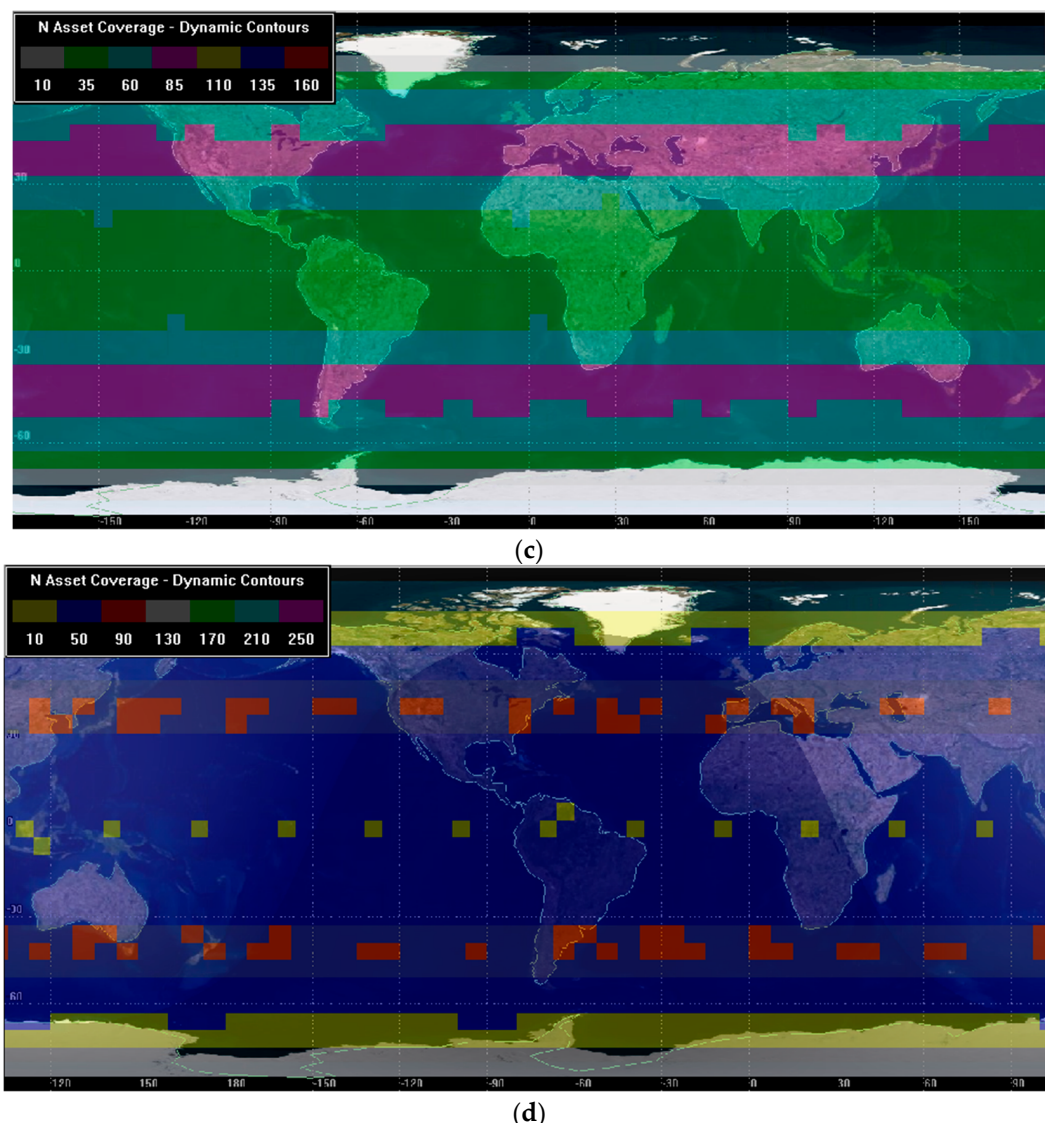


Figure 8. Comparison of coverage performance of Starlink and OneWeb constellation under different F.
 (a) OneWeb constellation, F = 1; (b) OneWeb constellation, F = 9; (c) Starlink constellation, F = 1;
 (d) Starlink constellation, F = 11.

Comparatively, it can be noted that setting the optimal phasing factor can significantly improve the constellation coverage performance, and for the majority of users distributed between 60° , Starlink showcases superior coverage performance than OneWeb.

Due to the superiority of the Starlink constellation coverage performance, the following analysis is mainly performed on the Starlink constellation with F = 11. The distance between any two satellites in the generated constellation model is observed to show the visibility relationship between any satellites in the form of a graph, and to describe the inter-stellar link AER characteristics, which is the key and basis for analyzing the constellation topology.

4.4. Visibility Analysis

Due to the fact that LEO satellites orbit the Earth at a high rate of speed, the latitude and longitude of the heterodyne satellites change in lockstep with them, affecting the network topology constructed by LISLs. As a result, the visibility analysis among the satellites is performed first in the simulation scenario. Since the geometric configuration of the Starlink constellation is symmetric, any satellite's geometric characteristics can be applied to represent the geometric characteristics of the remaining satellites that are

symmetric with it. We selected a satellite $S(2,1)$ as the research object in this paper to examine the visibility of LISLs between satellites in the same and different orbits within a 24 h period.

1. $S(2,1)$ and the satellites in the same orbit P_2

From Figure 9, it can be seen that there are sixteen satellites in the same orbit as $S(2,1)$ that are always visible during 24 h. The remaining satellites are not in the visual range due to the blockage of the Earth's sphere during the whole time, and no interplanetary link can be established. Therefore, it can be concluded that for any satellite $S(P_i, M_j)$, when $1 \leq i \leq 242 \leq j \leq 9$ is its forward eight satellites in the same orbit and $59 \leq j \leq 66$ is its backward eight satellites in the same orbit, these sixteen satellites can form permanent LISLs with a symmetric structure.

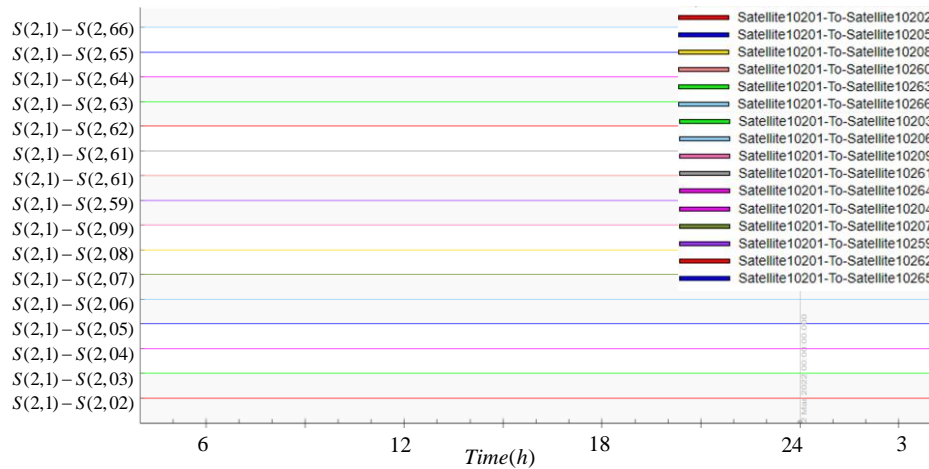


Figure 9. Visibility analysis of Co-orbiting satellites.

2. $S(2,1)$ and the satellites in the adjacent orbit P_1

As can be seen from Figure 10, due to the symmetrical structure of the constellation, there are 17 satellites in each of the two orbits adjacent to $S(2,1)$, P_1 and P_3 that can form permanent LISLs with them within 24 h. Therefore, there are 34 satellites that can render LISLs visible throughout the day, and their satellites are not visible throughout the day due to occlusion.

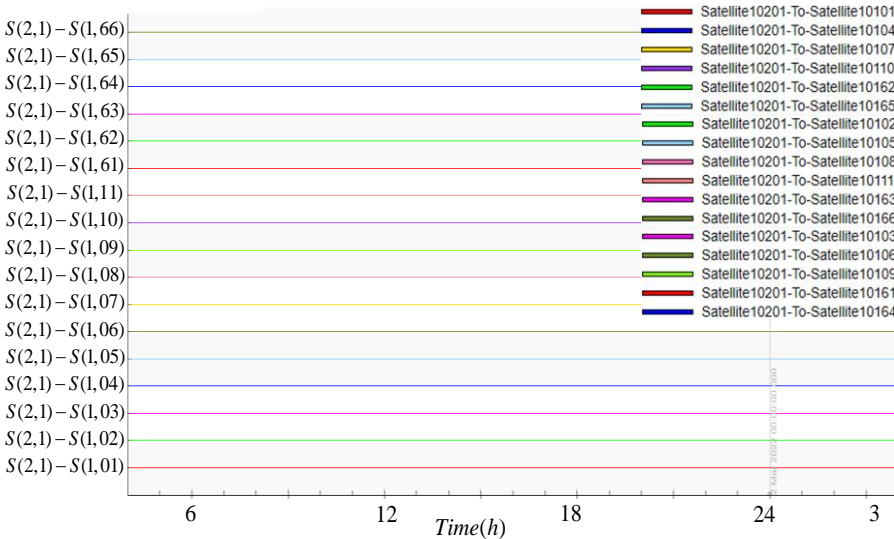


Figure 10. Visibility analysis of adjacent orbiting satellites.

3. visibility between $S(2, 1)$ and the satellites in the neighboring non-adjacent orbit P_5

As shown in Figure 11, it can be seen that on P_5 , there are ten satellites that are permanently visible 24 h, allowing for uninterrupted LISL establishment throughout the day; there are eight satellites which are intermittently visible on $S(2, 1)$, and the established LISLs may be interrupted. The number of such interruptions is represented in the figure as the number of intervals between the lines, e.g., 29 interruptions occur between $S(2, 1)$ and $S(5, 1)$ in a day; the rest of the satellites in this orbit, not shown in the figure, are unable to establish LISLs with $S(2, 1)$.

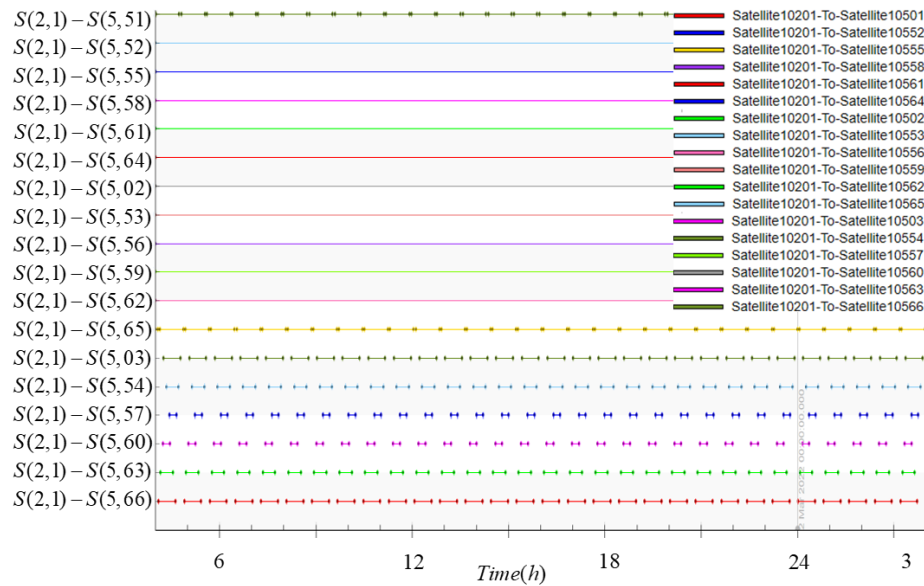


Figure 11. Visibility analysis of neighboring non-adjacent orbiting satellites.

4. $S(2, 1)$ and the satellites in more than three orbits apart P_6

The hetero-orbit is divided into adjacent orbits and neighboring non-adjacent orbits. From Figure 12, it can be seen that there are no satellites permanently visible to the selected satellite as long as they are separated by more than three orbits, either clockwise or counterclockwise. For the subject of this experiment, $S(2, 1)$, there are permanent LISLs with two adjacent orbits and four neighboring non-adjacent orbits, P_4 , P_5 , P_{23} and P_{24} .

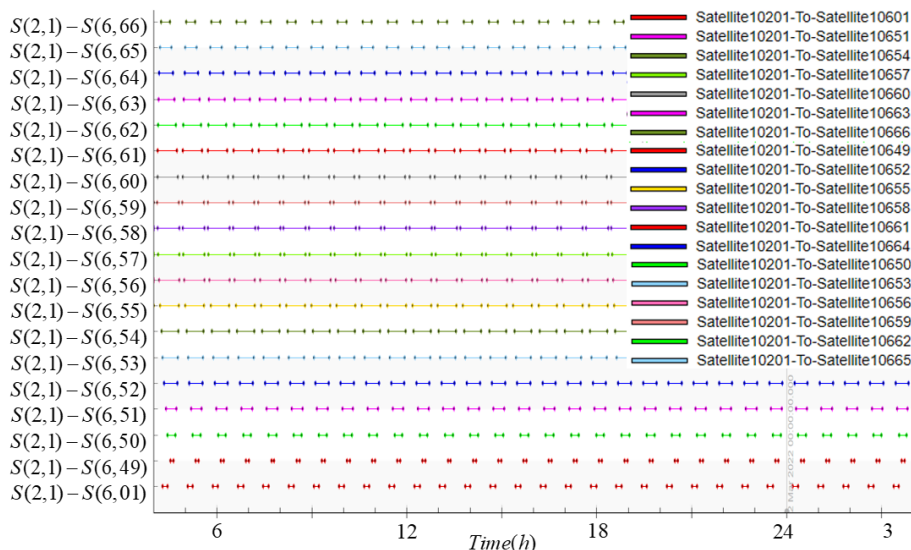


Figure 12. Satellite visibility analysis with more than 3 orbits apart.

4.5. AER Analysis

The AER characteristics of the Starlink constellation LISLs are analyzed, where A denotes the azimuth of the link, E denotes the elevation angle, and R denotes the interstellar distance, and it is discovered that LISLs in the same and different orbits exhibit distinct characteristics, which are correlated with the permanent LISLs calculated in the visibility analysis.

1. AER characteristics of the satellite $S(2,1)$ and the co-orbital link

From Figure 13, it can be seen that $S(2,1)$ has constant elevation and proximity angles and periodic azimuthal variation when $S(2,2)$ establishes co-orbital forward link; $S(2,1)$ has constant A, E, and R indicators when $S(2,66)$ establishes co-orbital backward link, which is due to the equal velocity vectors of satellite node motion within the same orbit and the their relative stationary relationship. This observation also indicates the permanent LISLs between visible satellites in the orbital plane.

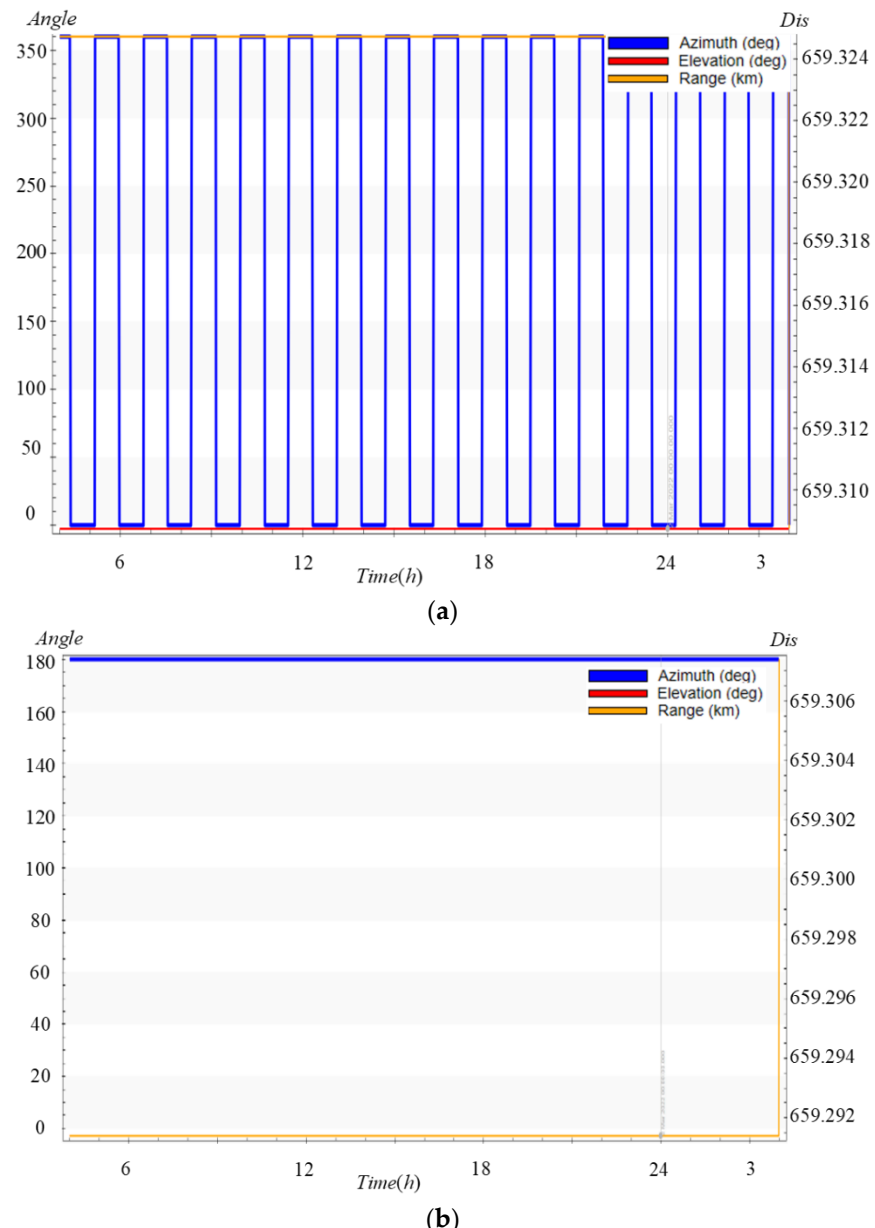


Figure 13. This is the schematic diagram of co-orbit link AER characteristic analysis. **(a)** Co-orbit forward link; **(b)** Co-orbit backward link.

2. AER characteristics of the satellite $S(2,1)$ and the heterodyne link

As shown in Figures 14–16, it can be seen that the LISLs established between $S(2,1)$ and $S(3,66)$ on adjacent orbits, whose link AER characteristics are all periodic and have similar trends, are still permanent LISLs; the temporary LISLs established between $S(2,1)$ and $S(5,1)$ on non-adjacent orbits can be seen to take non-continuous values, and when the visual distance is exceeded, the LISLs are disconnected, and no azimuth and elevation angles exist at this time; There are also a large number of temporary LISLs on $S(2,1)$ and $S(14,21)$ established on the intersecting orbit plane, with a longer interval between link disconnections. While the LISLs between the crossing orbit planes may provide a backup option for link reconstruction in the event of a network node failure by increasing the topology structure's redundancy, there are also numerous challenges to resolve in developing hardware functions.

The link length is a critical parameter in the geometric characterization of intersatellite links, as it affects the link's transmission efficiency, time delay, throughput, and other indexes, and the AER characterization reveals the relevant laws to a certain extent. After analyzing the AER characteristics of LISLs established between co-orbital and heterodyne orbits, it is concluded in this paper that when LISLs are established with permanently visible satellites, the link AER characteristics exhibit periodic changes and take continuous values, whereas LISLs established with intermittently visible satellites break the link when out of the visible range. The change in azimuth affects the on/off state of LISLs, and the time delay introduced by the link communication varies with distance. is similar for both co-orbital and heterodyne LISLs, which reflects the geometric characteristic of the Starlink constellation, which is a uniformly distributed LEO layer, in accordance with the Delta constellation characteristics at an orbital altitude of 550 km.

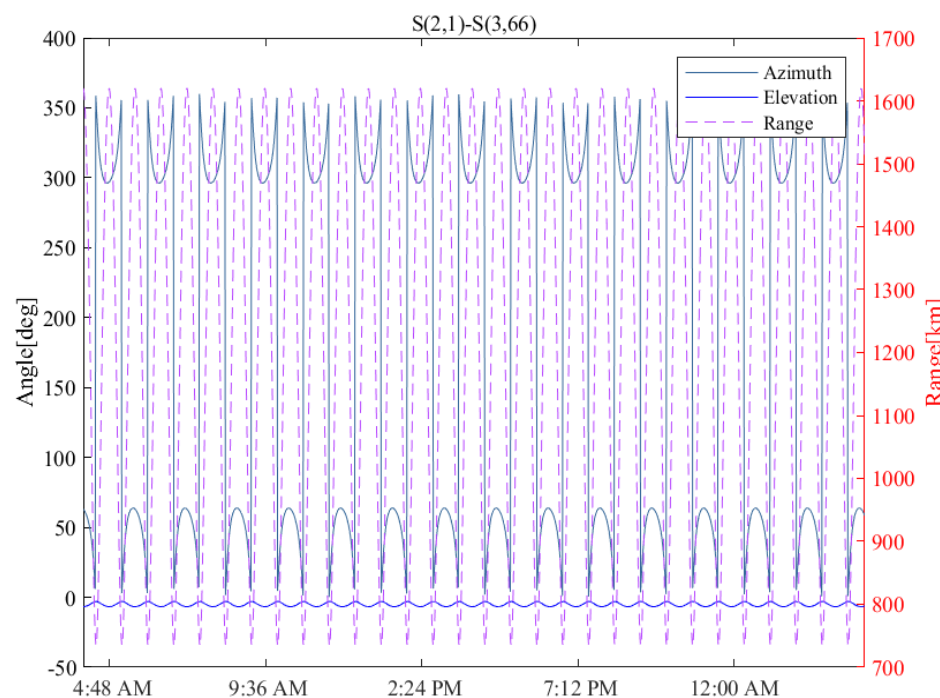


Figure 14. Characterization of the adjacent orbital link AER.

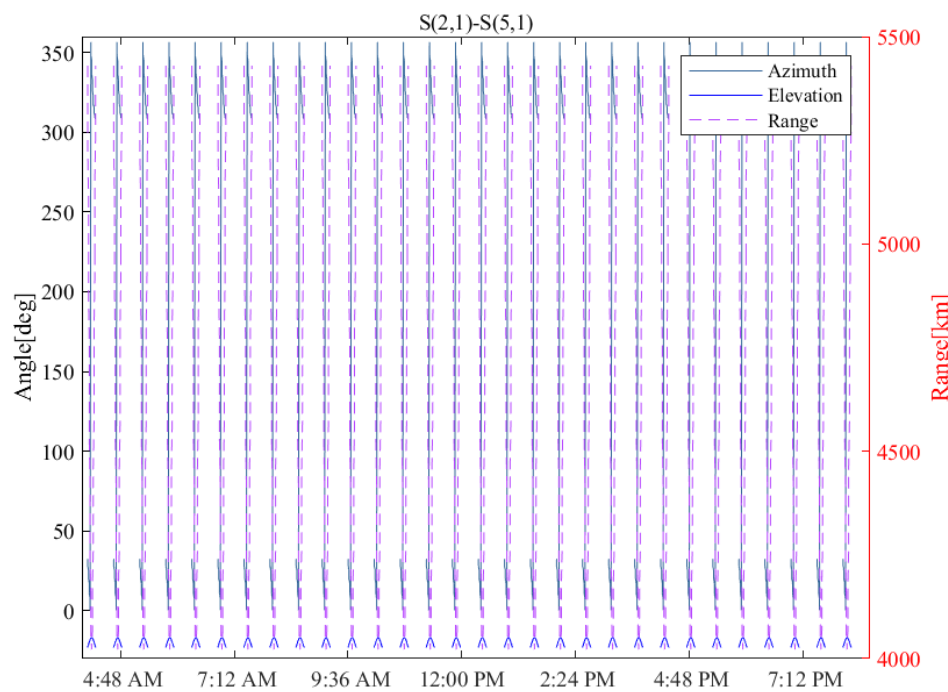


Figure 15. Neighboring non-adjacent orbital link AER characterization diagram.

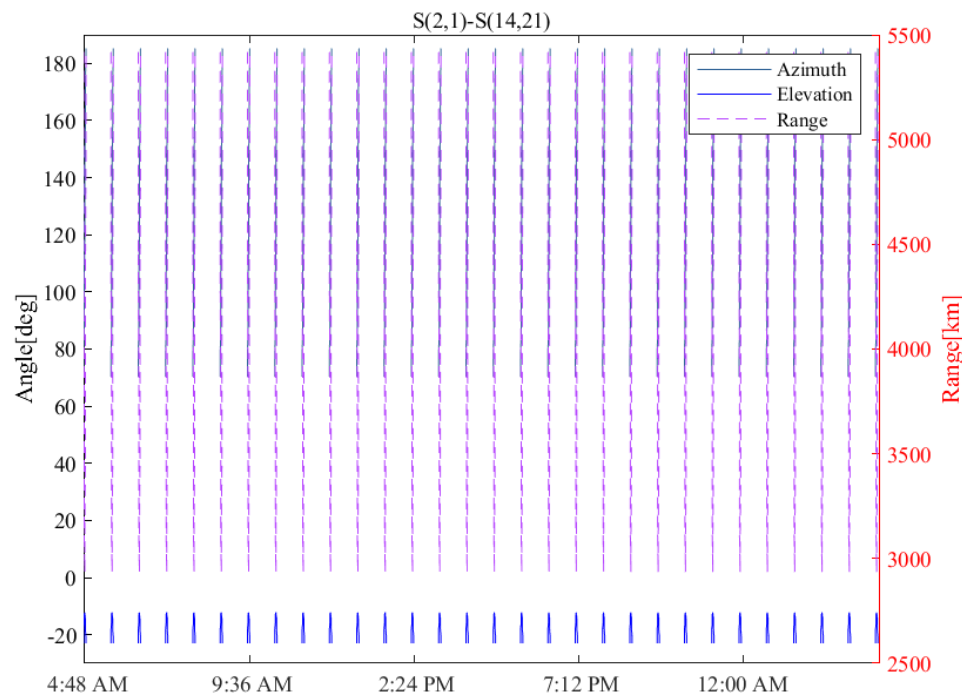


Figure 16. Crossing orbital link AER characterization diagram.

4.6. Number of LISLs in Different Distance Ranges

- Permanent LISLs

The pattern of persistent LISLs is evidenced by both intersatellite visibility and AER characterization. For data collation, data were obtained from the simulation distance analysis report, and the number of permanent LISLs in various visibility ranges was searched for using the different distance ranges of LISLs existing between the same orbit as the classification criteria, as shown in Table 3.

Table 3. Number of permanent LISLs at different visual distance ranges.

LISLs Range (km)	Intra-OP	AOPLs	NOPLs	Total
659	2	0	0	2
1317	4	0	0	2
1972	4	2	0	6
2622	4	6	0	10
5016	16	34	44	94

In an environment without water vapor, the lowest atmospheric layer starts at about 80 km above the Earth's surface, which coincides with the minimum height of LISLs above the surface. The radius of the Earth at the equator is 6378 km, and in the Starlink constellation, there are $R = 6378$ km, $h = 550$ km, $H = 80$ km, and the maximum visible distance between satellites is calculated by combining Equation (13) with $x = 5016$ km. Using a single satellite as an example, under the condition of maximum visibility range of 5016 km, this satellite may establish up to 94 permanent LISLs, including 16 intra-same-orbit cases, 34 adjacent inter-orbit cases, and 44 neighboring non-adjacent inter-orbit cases.

- Temporary LISLs

As shown in Table 4, the satellite $S(2, 1)$ can establish 30 temporary LISLs with $S(5, 1)$ in non-adjacent orbits within 24 h with an average duration of 1895s, where the range of LISLs for $S(2, 1)$ is about 1972 km, within which $S(2, 1)$ can also establish similar temporary links between four adjacent orbital planes.

Table 4. Temporary LISLs between $S(2, 1)$ and $S(5, 1)$.

Access	Start Time	Stop Time	Duration (s)
1	04:06:26.497	04:38:02.065	1895.568
2	04:54:14.226	05:25:49.799	1895.573
3	05:42:01.955	06:13:37.525	1895.569
4	06:29:49.683	07:01:25.256	1895.573
5	07:17:37.413	07:49:12.985	1895.573
6	08:05:25.139	08:37:00.710	1895.570
7	08:53:12.869	09:24:48.441	1895.572
8	09:41:00.599	10:12:36.171	1895.572
9	10:28:48.324	11:00:23.896	1895.572
10	11:16:36.054	11:48:11.626	1895.572
11	12:04:23.786	12:35:59.355	1895.570
12	12:52:11.510	13:23:47.083	1895.573
13	13:39:59.244	14:11:34.812	1895.568
14	14:27:46.971	14:59:22.543	1895.572
15	15:15:34.697	15:47:10.270	1895.573
16	16:03:22.430	16:34:57.998	1895.568
17	16:51:10.157	17:22:45.728	1895.571
18	17:38:57.883	18:10:33.456	1895.573
19	18:26:45.617	18:58:21.187	1895.570
20	19:14:33.345	19:46:08.916	1895.571
21	20:02:21.073	20:33:56.643	1895.569
22	20:50:08.803	21:21:44.376	1895.573
23	21:37:56.531	22:09:32.102	1895.571
24	22:25:44.261	22:57:19.829	1895.568
25	23:13:31.990	23:45:07.563	1895.573
26	00:01:19.719	00:32:55.288	1895.570
27	00:49:07.447	01:20:43.019	1895.572
28	01:36:55.176	02:08:30.749	1895.573
29	02:24:42.903	02:56:18.474	1895.571
30	03:12:30.632	03:44:06.204	1895.572

When the range of LISLs reaches a certain level, a large number of temporary LISLs appear in addition to the permanent LISLs, and the number of temporary links generally increases positively along with the range of inter-satellite LISLs. The data indicate that temporary LISLs exist primarily between cross orbital planes, and mainly when satellites operate to the extent that two satellites are within the range of temporary LISLs. There will be intermittent temporary links in different time periods that serve as an auxiliary role to the connection of permanent links, maintaining the stability of the communication network, and that within the maximum range of LISLs, i.e., 5016 km, a satellite can form 293 temporary links within the span of 24 h.

4.7. Link Connection Policy

According to the analysis above, inter-satellite links can be classified in three categories as permanently visible, intermittently visible, or invisible. Satellites in the same orbit as well as those in adjacent orbits have only two permanent states of visibility and invisibility. If the inter-satellite distance is moderate and does not exceed the maximum visible distance, it is within the visible range, allowing for the establishment of a permanent link. Satellites in non-adjacent orbits have three states of visibility, and when the interplanetary link is disrupted several times, it is referred to as a dynamic link, since it is frequently disconnected and reconnected [26].

The AER characteristics of co-orbital links indicate that, for any satellite, the satellite nodes located in the same orbital plane are relatively stationary, suggesting the presence of a permanent link of fixed length with visible satellites in the same orbital plane that is always connected, i.e., the co-orbital links have equal survival time. Consequently, two of each satellite's four intersatellite links are assigned to connect two adjacent satellites in the same orbit, while the forward and backward connections within the same orbit are kept in a constant direction, allowing for hop-by-hop data transmission along the same orbit or in the opposite direction.

According to the AER characteristics of the heterodyne link, it is understood that the visible satellites in two adjacent orbits are permanently visible and linked, while the remaining satellites in non-adjacent orbits exist in two scenarios: (1) a permanently visible link can be established between satellites, but the distance between is too great, resulting in an excessive time delay; (2) the distance between satellites is closest at a certain moment, but the visible time is too short, and as the satellites continue to operate, there will be frequent disruptions in the cycle, frequent disconnection and reconnection of the link, resulting in an excessive number of link-switching times. Combining the two scenarios above, it is evident that the best option is to establish a link with an adjacent orbiting visible satellite. The adjacent inter-orbit link is shorter in distance than the non-adjacent orbit permanent link; unlike the non-adjacent orbit closest satellite, the adjacent inter-orbit satellite does not need to switch the link during the cycle, making the link more stable. Meanwhile, the adjacent inter-orbit link can transmit data hop-by-hop along the east-west direction, and the phasing factor selection will slightly deviate the orbit from the positive east-west direction, generating a larger transmission path.

In summary, as shown in Figure 17, a static topology of 1584 satellites in the first phase of the Starlink constellation can be constructed, with the arrow indicating the direction of the satellite. As the inter-satellite distance range increases, satellites are able to establish more stable permanent links. If the satellite operation period is divided into equally spaced time slices, then a similar static topology exists within each time slice, and a large number of different temporary links exist within each time slice as time progresses. On the grounds of the periodicity and predictability of the nearest satellites over time, a strategy of dividing the number of time slices based on the number of satellites per orbit can be considered, and the satellite connectivity of all satellites within a time slice can be directly derived from the resulting LISLs law, significantly reducing the computational effort associated with the topology building process.

Considering that not all launched satellites approach orbit and that some fail due to electromagnetic storms and other factors, it is also necessary to study the visibility and number law of LISLs in various time slices for link reconfiguration under dynamic topology. However, provided the laser beam's narrow beam width and the differing relative velocities of the two satellites that connect the intersecting orbital planes, establishing some temporary LISLs is challenging, and a more precise ATP system needs to be developed. In the future, the failure of a single satellite can also be utilized as a case study. The law analyzed in this paper is presented to probe a link reconstruction algorithm with a high degree of connectivity and a low delay, as well as the optimal routing protocol based on the shortest path principle.

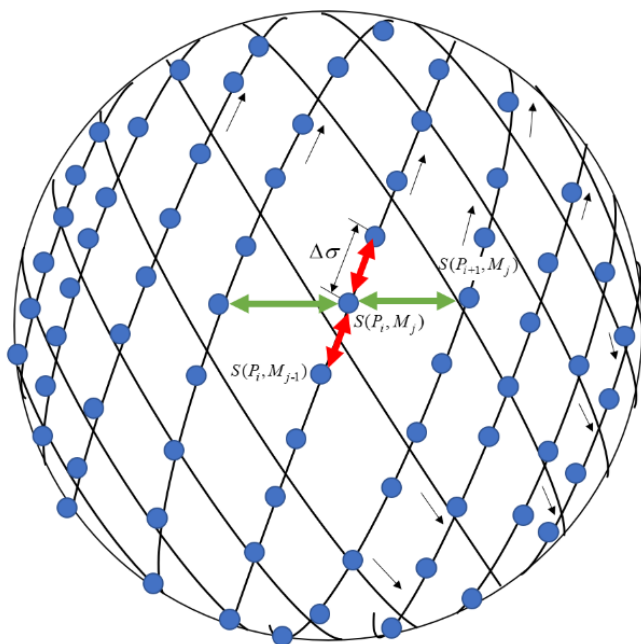


Figure 17. Starlink constellation static topology.

5. Conclusions

The term “inter-satellite link” refers to a wireless connection between two satellites in a network that acts as a conduit for data exchange between satellite nodes. The spatial location and duration of inter-satellite links of satellites in the mega-constellation are utilized to classify and number various types of LISLs between the constellation’s satellites, and a basic model for satellite network topology analysis is created in this paper.

Whereupon, with the usage of the optimization algorithm, the optimal phasing factors of the OneWeb and Starlink constellations with a large number of deployed satellites are determined to be $F = 9$ and $F = 11$, respectively. The comparison group is then set up, followed by the OneWeb constellation with $F = 1$ and $F = 9$, the Starlink constellation with $F = 1$ and $F = 11$, and the global coverage multiplicity map is obtained to demonstrate the efficacy of the F optimization algorithm proposed in this paper. Between the latitudes of 60° north and south, the coverage performance of the Starlink constellation is superior to that of the OneWeb constellation.

Based on the coverage performance comparison results, the Starlink constellation with $F = 11$ is selected for the visibility and AER analysis of the LISLs, which is used to verify the link-building thresholds for co-orbital and hetero-orbital links, and the number of LISLs in different distance ranges is subsequently derived from the inter-satellite distance. Finally, based on the visibility and the number of links, the laser link connection strategy between co-orbital and hetero-orbital satellites is summarized, with the objective of theoretically constructing the static topology of 1584 satellites in the first phase of Starlink constellation

deployment and laying the foundations for the constellation's dynamic routing design and analysis.

According to the constructed topology, when the Starlink constellation is observed in any area above the Earth, we can find out that half of the constellation's satellites orbit southeast, while the other half orbit northeast. These mission satellites generate a large number of intermittent LISLs in different directions among the intersecting satellites. A satellite can establish up to 94 permanent LISLs and 293 temporary cross-orbital interplane links with other satellites within 24 h under the condition of the maximum LISL distance range of 5016 km. While this connection state cannot remain for long, such links are critical for increasing constellation redundancy and survivability, improving routing options to reduce path delays, and more. Therefore, determining the regularity of the inter-orbital inter-satellite link at various times during the cycle is critical for increasing the flexibility of network communication.

Supplementary Materials: The following supporting information can be downloaded at: <https://www.space-track.org/#catalog> (accessed on 15 April 2022).

Author Contributions: Conceptualization, Q.Z., H.T., Y.C. and X.L.; methodology, Q.Z. and Y.C.; software, Q.Z.; validation, H.T.; formal analysis, Q.Z.; investigation, Q.Z.; resources, X.L., Q.Z. and H.T.; writing—original draft preparation, Q.Z.; writing—review and editing, Q.Z., H.T.; visualization, Q.Z.; supervision, Y.C. and Q.Z. All authors have read and agreed to the published version of the manuscript.

Funding: This research received no external funding.

Data Availability Statement: All data generated or analyzed during this study are included in this article.

Acknowledgments: I would like to thank everyone who helped with this paper, especially my supervisor, and my colleagues who made this paper possible.

Conflicts of Interest: The authors declare no conflict of interest.

References

1. Boccardi, F.; Heath, R.W.; Lozano, A.; Marzetta, T.L.; Popovski, P. Five Disruptive Technology Directions for 5G. *IEEE Commun. Mag.* **2014**, *52*, 74–80. [[CrossRef](#)]
2. Kodheli, O.; Lagunas, E.; Maturo, N.; Sharma, S.K.; Shankar, B.; Montoya, J.F.M.; Duncan, J.C.M.; Spano, D.; Chatzinotas, S.; Kisseleff, S.; et al. Satellite Communications in the New Space Era: A Survey and Future Challenges. *IEEE Commun. Surv. Tutor.* **2021**, *23*, 70–109. [[CrossRef](#)]
3. Orabi, M.; Khalife, J.; Kassas, Z.M. Opportunistic Navigation with Doppler Measurements from Iridium Next and Orbcomm LEO Satellites. In Proceedings of the 2021 IEEE Aerospace Conference (50100), Big Sky, MT, USA, 6 March 2021; pp. 1–9.
4. Osoro, O.B.; Oughton, E.J. A Techno-Economic Framework for Satellite Networks Applied to Low Earth Orbit Constellations: Assessing Starlink, OneWeb and Kuiper. *IEEE Access* **2021**, *9*, 141611–141625. [[CrossRef](#)]
5. Brian, D. Weimer Application for Fixed Satellite Service by WorldVu Satellites Limited, Debtor-in-Possession [SAT-MPL-20200526-00062]. Available online: <https://fcc.report/IBFS/SAT-MPL-20200526-00062> (accessed on 27 May 2022).
6. del Portillo, I.; Cameron, B.G.; Crawley, E.F. A Technical Comparison of Three Low Earth Orbit Satellite Constellation Systems to Provide Global Broadband. *Acta Astronaut.* **2019**, *159*, 123–135. [[CrossRef](#)]
7. Yu, Q.; Wang, J.; Bai, L. Architecture and Critical Technologies of Space Information Networks. *J. Commun. Inf. Netw.* **2016**, *1*, 1–9. [[CrossRef](#)]
8. Yan, J.; Xing, L.; Wang, P.; Sun, L.; Chen, Y. A Scheduling Strategy to Inter-Satellite Links Assignment in GNSS. *Adv. Space Res.* **2021**, *67*, 198–208. [[CrossRef](#)]
9. Zeng, L.; Lu, X.; Bai, Y.; Liu, B.; Yang, G. Topology Design Algorithm for Optical Inter-Satellite Links in Future Navigation Satellite Networks. *GPS Solut.* **2022**, *26*, 1–16. [[CrossRef](#)]
10. Chen, Q.; Giambene, G.; Yang, L.; Fan, C.; Chen, X. Analysis of Inter-Satellite Link Paths for LEO Mega-Constellation Networks. *IEEE Trans. Veh. Technol.* **2021**, *70*, 2743–2755. [[CrossRef](#)]
11. Guan, M.; Xu, T.; Gao, F.; Nie, W.; Yang, H. Optimal Walker Constellation Design of LEO-Based Global Navigation and Augmentation System. *Remote Sens.* **2020**, *12*, 1845. [[CrossRef](#)]
12. Chaudhry, A.U.; Yanikomeroglu, H. Laser Intersatellite Links in a Starlink Constellation: A Classification and Analysis. *IEEE Veh. Technol. Mag.* **2021**, *16*, 48–56. [[CrossRef](#)]

13. Liu, S.; Yang, J.; Guo, X.; Sun, L. Inter-Satellite Link Assignment for the Laser/Radio Hybrid Network in Navigation Satellite Systems. *GPS Solut.* **2020**, *24*, 49. [[CrossRef](#)]
14. Yu, X.; Tong, S.; Zhang, L.; Dong, Y.; Zhao, X.; Qiao, Y. 1023 Mcps Laser Pseudo-Code Ranging System with 033 Mm (1σ) Pseudo-Range Measurement Precision. *Appl. Opt.* **2017**, *56*, 5342. [[CrossRef](#)] [[PubMed](#)]
15. Long, M.J. Pointing Acquisition and Tracking Design and Analysis for CubeSat Laser Communication. Ph.D. Thesis, Crosslinks, Massachusetts Institute of Technology, Cambridge, MA, USA, 2018.
16. Boriboon, A.; Pongpadpinit, S. Optimized Routing Protocol for Broadband Hybrid Satellite Constellation Communication IP Network System. *J. Wirel. Commun. Netw.* **2016**, *2016*, 120. [[CrossRef](#)]
17. McDowell, J.C. The Low Earth Orbit Satellite Population and Impacts of the SpaceX Starlink Constellation. *Astrophys. J. Lett.* **2020**, *892*, L36. [[CrossRef](#)]
18. Roth, M.; Brandt, H.; Bischl, H. Implementation of a Geographical Routing Scheme for Low Earth Orbiting Satellite Constellations Using Intersatellite Links. *Int. J. Satell. Commun. Netw.* **2021**, *39*, 92–107. [[CrossRef](#)]
19. Chen, Q.; Yang, L.; Liu, X.; Guo, J.; Wu, S.; Chen, X. Multiple Gateway Placement in Large-scale Constellation Networks with Inter-satellite Links. *Int. J. Satell. Commun. Netw.* **2021**, *39*, 47–64. [[CrossRef](#)]
20. Lee, Y.; Choi, J.P. Connectivity Analysis of Mega-Constellation Satellite Networks with Optical Intersatellite Links. *IEEE Trans. Aerosp. Electron. Syst.* **2021**, *57*, 4213–4226. [[CrossRef](#)]
21. Wang, F.; Jiang, D.; Qi, S. An Adaptive Routing Algorithm for Integrated Information Networks. *China Commun.* **2019**, *16*, 195–206. [[CrossRef](#)]
22. Amanor, D.N.; Edmonson, W.W.; Afghah, F. Intersatellite Communication System Based on Visible Light. *IEEE Trans. Aerosp. Electron. Syst.* **2018**, *54*, 2888–2899. [[CrossRef](#)]
23. Bhattacherjee, D.; Singla, A. Network Topology Design at 27,000 Km/Hour. In Proceedings of the 15th International Conference on Emerging Networking Experiments and Technologies, Orlando, FL, USA, 9–12 December 2019; pp. 341–354.
24. Satellite Database. Union of Concerned Scientists. Available online: <https://www.ucsusa.org/resources/satellite-database> (accessed on 9 July 2022).
25. Li, H.; Li, D.; Li, Y. A Multi-Index Assessment Method for Evaluating Coverage Effectiveness of Remote Sensing Satellite. *Chin. J. Aeronaut.* **2018**, *31*, 2023–2033. [[CrossRef](#)]
26. Chengzhuo, W.; Suyang, L.; Xiye, G.; Jun, Y. Dynamic Optimization of Laser Inter-Satellite Link Network Topology Based on Genetic Algorithm. In Proceedings of the 2019 14th IEEE International Conference on Electronic Measurement & Instruments (ICEMI), Changsha, China, 1–3 November 2019; pp. 1331–1342.